INTERFACE FOCUS

royalsocietypublishing.org/journal/rsfs

Research

Cite this article: Routzong MR, Moalli PA, Maiti S, De Vita R, Abramowitch SD. 2019 Novel simulations to determine the impact of superficial perineal structures on vaginal delivery. *Interface Focus* **9**: 20190011. http://dx.doi.org/10.1098/rsfs.2019.0011

Accepted: 7 May 2019

One contribution of 13 to a theme issue 'Bioengineering for women's health, volume 1: female health and pathology'.

Subject Areas:
biomechanics, bioengineering

Keywords:
biomechanics, finite-element model, perineal body, pubovisceral muscle, superficial perineal structures, vaginal delivery

Author for correspondence:
Megan R. Routzong
e-mail: mer136@pitt.edu

Electronic supplementary material is available online at https://doi.org/10.6084/m9.figshare.c.4505255.

THE ROYAL SOCIETY PUBLISHING

Novel simulations to determine the impact of superficial perineal structures on vaginal delivery

Megan R. Routzong[1], Pamela A. Moalli[2], Spandan Maiti[3], Raffaella De Vita[4] and Steven D. Abramowitch[1]

[1]Translational Biomechanics Laboratory, Department of Bioengineering, Swanson School of Engineering, [2]Magee-Womens Research Institute, Magee-Womens Hospital, and [3]Department of Bioengineering, Swanson School of Engineering, University of Pittsburgh, Pittsburgh, PA, USA
[4]STRETCH Lab, Department of Biomedical Engineering and Mechanics, Virginia Tech, Blacksburg, VA, USA

MRR, 0000-0001-5551-1156; RDV, 0000-0003-3157-9409; SDA, 0000-0001-7762-7723

This study's aim was to determine whether the inclusion of superficial perineal structures in a finite-element simulation of vaginal delivery impacts the pubovisceral muscle and perineal body, two common sites of birth-related injury. The hypothesis, inferred from prevailing literature, was that these structures would have minimal influence (differences less than $\pm 10\%$). Two models were made using the Visible Human Project's female cadaver to create a rigid, fixed pelvis, musculature held by spring attachments to that pelvis, and a rigid, ellipsoidal fetal head prescribed with an inferior displacement to simulate delivery. Injury site stretch ratios and fetal head and perineal body displacements and angles of progression were compared between the Omitted Model (which excluded the superficial perineal structures as is common practice) and the Included Model (which included them). Included Model stretch ratios were $+107\%$, -9.84% and -14.6% compared to Omitted Model perineal body and right and left pubovisceral muscles, respectively. Included Model peak perineal body inferior displacement was $+72.5\%$ greater while similar anterior–posterior displacements took longer to reach. These results refute our hypothesis, suggesting superficial perineal structures impact simulations of vaginal delivery by inhibiting perineal body anterior–posterior displacement, which stretches and inferiorly displaces the perineal body.

1. Introduction

Injury to the soft tissues that provide pelvic organ support during vaginal delivery can lead to the development of pelvic floor disorders decades later [1,2]. Previous finite-element simulations predicted pubovisceral muscle enthesis injury during vaginal delivery, an injury which has been identified with medical imaging in 18% of parous women after delivery [3,4]. Meanwhile, other studies have found that 65.8% of parous women experience perineal body disruption during vaginal delivery [5]. In existing finite-element models of childbirth, however, the maximum stretch values at the pubovisceral muscle are approximately 10% larger than those at the perineal body [3]. If stretch positively correlates with injury, then these numbers do not coincide with the relative prevalence of these injuries observed clinically. Thus, a clear understanding of stretching during vaginal delivery is critical to simulating mechanisms of injury.

Finite-element models of vaginal delivery commonly include only the levator ani muscles, the major components of pelvic organ support that maintain the genital hiatus, which may be adequate for certain research questions [6–9]. However, they generally exclude superficial perineal structures—such as the bulbocavernosus, ischiocavernosus and deep and superficial transverse perinei—striated muscles with high connective tissue content that are superficial to the levator ani and intersect at the perineal body [2,10] (figure 1). These structures are

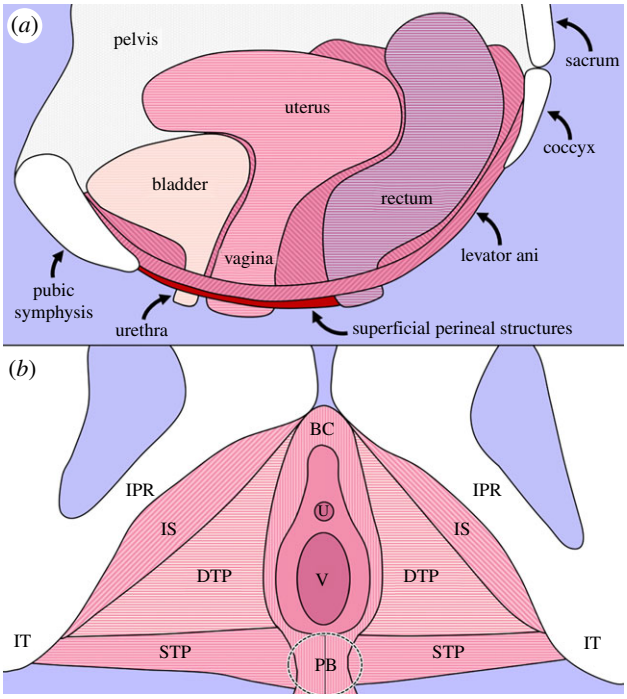

Figure 1. An illustration of (*a*) the female pelvis from the midsagittal plane with the region where the superficial perineal structures are located emphasized in red and (*b*) the superficial perineal structures (the bulbocavernosus (BC), ischiocavernosus (IS), deep transverse perinei (DTP) and superficial transverse perinei (STP)) in detail. Shown for reference are the inferior pubic rami (IPR), urethra (U), vagina (V), ischial tuberosities (IT) and the perineal body (PB). (Online version in colour.)

commonly omitted from simulations as they are difficult to segment from imaging, and, based on visual inspection, seem to be mechanically insignificant compared to the levator ani [11]. Anatomically, superficial perineal structures resist caudal motion of the perineal body, meaning their exclusion may allow non-physiological movement of maternal soft tissues [10,11]. Our objective was to determine the impact of these superficial perineal structures on the stretch ratios measured in the pubovisceral muscle and perineal body during a simulation of vaginal delivery. The hypothesis, based on the assumptions of previous literature, was that they would have minimal impact (differences less than $\pm 10\%$).

2. Material and methods

2.1. Geometry processing and meshing

The geometry of the finite-element model developed in this study was composed of six parts: the maternal bony pelvis (right and left pelvic bones, sacrum, and coccyx), the maternal musculature (which includes the levator ani and superficial perineal muscles), and the fetal head (figure 2). The muscles and bony pelvis were manually segmented from frozen cryosection images (with a 0.33 mm slice thickness) of the female cadaver (parous, deceased at age 59 from a heart attack) from the Visible Human Project (US National Library of Medicine, Bethesda, MD, USA), the use of which required a licence but not consent or IRB approval. This anatomy was chosen as the unusually thin slice thickness allowed for visualization and segmentation of the difficult to identify superficial perineal structures in greater detail than magnetic resonance imaging or computed tomography is currently capable of. These geometries were then manually smoothed in 3D-Coat v.4.1.16 (Pilgway, Kiev, Ukraine) to remove aliasing, the step-like formations created around the edges of shapes due to discrete image slices, by filling the gaps and smoothing the peaks between slices. This biased smoothing approach was chosen as global smoothing techniques led to the decimation of relatively thinner regions of these complex geometries.

The fetal head was represented as an ellipsoid created within PreView v1.19.0 (University of Utah, Salt Lake City, UT, USA) and therefore did not require smoothing. The dimensions of the fetal head were approximated based on clinical averages, but the width was limited by the shape of the maternal bony pelvis—in particular, the interspinous distance (the distance between the ischial spines). This resulted in a fetal head circumference of 254.6 mm, which is more representative of a term fetus at 27–29 weeks or a preterm fetus at 25.5–31.5 weeks rather than a term fetus at 40 weeks [12–14]. This was the largest fetal head possible given the material properties and boundary conditions of this first-generation model (described in the following section).

Triangle surface meshes were created for all maternal geometries using Instant Meshes (Interactive Geometry Lab ETH Zurich, Zurich, Switzerland), as forming a surface of triangular elements is computationally easier for complex geometries. These meshes were then imported into PreView where volume meshes composed of tetrahedral elements, which are made of four triangular faces, were generated for the deformable maternal geometries (the coccyx and musculature) using the TetGen function. The hexahedral volume mesh of the fetal head was also generated within PreView. In total, the pelvic bones and sacrum consisted of 43 190 triangular elements, the coccyx had 1042 four-noded tetrahedral elements, the fetal head had 27 648 eight-noded hexahedral elements, and the muscle had 518 542 four-noded tetrahedral elements which were determined as a sufficient mesh density by a mesh convergence study (figure 3). The mesh was considered converged once increasing the density consistently resulted in corresponding strain value measurements with differences of less than 5%, which is where the mesh convergence curve plateaus.

2.2. Material properties and boundary conditions

The pelvic bones and sacrum were assigned as rigid bodies and fixed in all degrees of freedom, so they could not translate or rotate. The coccyx was deformable only to achieve the desired boundary conditions (sagittal rotation about a single point) but was given a stiffness 10 times greater than that of the muscle so that it essentially behaved as a rigid body. All maternal muscles were modelled as a single, isotropic, homogeneous, nearly incompressible, neo-Hookean, three-dimensional continuum. Since representative values of the material parameters for many of the involved tissues are unknown, especially at the time of delivery, material properties were selected to be the same for all muscles. The perineal body was represented as the medial region between the ends of the bulbocavernosus and superficial transverse perinei muscles, while the pubovisceral muscle was the medial portion of the levator ani near the attachment sites to the superior pelvic rami. The fetal head was a rigid body; free to translate in any direction during a prescribed downward (z) displacement of 60 mm, but fetal head crowning for both models was reached long before this displacement was achieved. All fetal head rotations were fixed with an initial orientation chosen to maximize the overall size of the fetal head but minimize the circumference passing through the maternal bony pelvis.

Connective tissues were simulated as springs defined by force–displacement curves with a stiffness of 0 N mm^{-1} in compression, meaning they did not resist compressive loads. The connective tissues of the superficial perineal structures simulated included the attachments from the ischiocavernosus and bulbocavernosus muscles to the inferior pubic rami, from the superficial transverse perinei muscles to the ischial tuberosities, and from the deep transverse perinei muscles to the inferior pubic rami

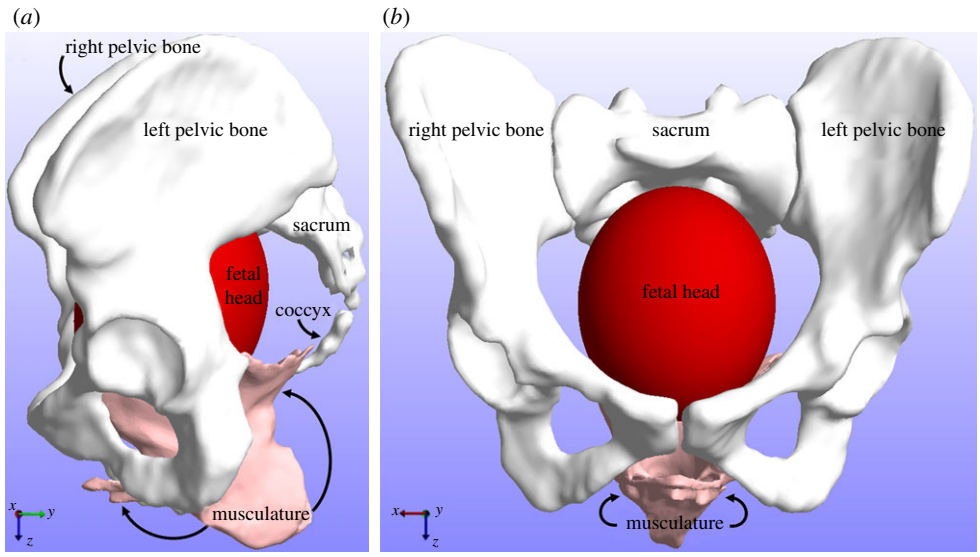

Figure 2. (*a*) A sagittal view and (*b*) coronal view of the six separate geometries included in these finite-element simulations. The maternal bony pelvis is shown in white, the maternal musculature in pink, and the fetal head in red. (Online version in colour.)

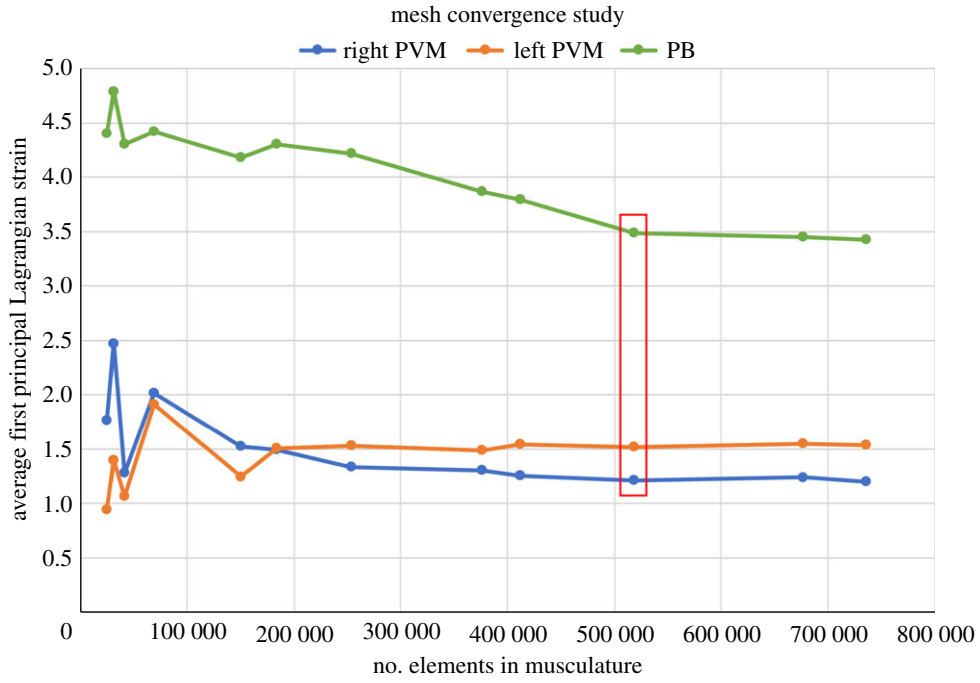

Figure 3. The results of our mesh convergence study demonstrating that convergence was reached for the strain outputs at all three anatomical regions of interest when the maternal musculature was composed of approximately 519 000 tetrahedral elements. PVM, pubovisceral muscle; PB, perineal body. (Online version in colour.)

(figure 4*a*,*c*). Other connective tissues simulated were the attachments from the sacrum to the coccyx (representing the sacrococcygeal ligaments), from the posterior levator ani to the sacrum (representing the anococcygeal raphe/levator plate), from the posterior levator ani to the tip of the coccyx (representing the anococcygeal raphe/levator plate and anococcygeal ligament), from the levator ani to the superior pubic rami (representing the origin of the arcus tendinous fascia pelvis and anterior portion of the arcus tendinous levator ani), and from the levator ani to the ischial spines (representing the insertion of the arcus tendinous fascia pelvis [15] (figure 4*b*,*d*). Initially, all connective tissue stiffness values in tension were equal and then altered iteratively, where the final values selected restricted non-physiological movement (figure 4*e*). Assuming material properties are roughly equivalent across these connective tissues, using structural properties (i.e. stiffness) ensures that thicker tissues, represented with more spring attachments, will provide more resistance to stretch. As resulting stresses were not the focus of this study, neither pressures nor forces were prescribed, and the mechanical behaviour of these tissues remains undefined for women at term, relative stiffness and material parameter values were assigned to recreate the gross mechanical behaviour of delivery while avoiding additional computational complexities (such as element locking) and non-physiological motion.

2.3. Finite-element model description

To allow appropriate movement of the muscles and fetal head, contact conditions were created between the fetal head and maternal musculature, fetal head and maternal bony pelvis, and bony pelvis and musculature where their surfaces were expected or found to meet. Contact between all bodies was assumed to be frictionless sliding and was enforced with a penalty parameter determined by trial and error and then adjusted as part of the

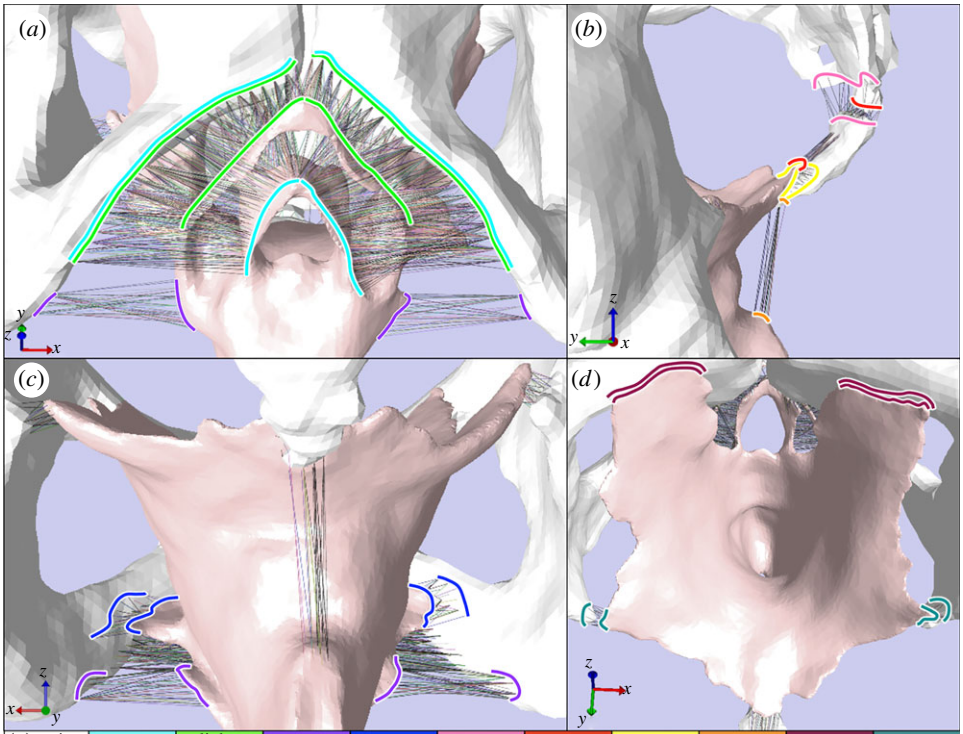

(e) spring colour	light blue	light green	purple	dark blue	pink	red	yellow	orange	maroon	teal
stiffness (N mm^{-1})	16.5	16.5	16.5	16.5	123.75	66	49.5	49.5	123.75	66

Figure 4. Images highlighting the (*a*) superficial connective tissues from an inferior, anterior view, (*b*) posterior connective tissues from a left, sagittal view, (*c*) remaining superficial tissues from a posterior, coronal view, (*d*) superior connective tissues from a superior view and (*e*) stiffness values colour coded with their corresponding attachment site outlines. Shown explicitly are the connective tissue components of the bulbocavernosus (light blue), ischiocavernosus (light green), superficial transverse perinei (purple) and deep transverse perinei (dark blue) muscles and the following connective tissues: sacrococcygeal ligaments (pink), anococcygeal raphe/levator plate (red and yellow), anococcygeal ligament (orange), origin of the arcus tendinous fascia pelvis and anterior portion of the arcus tendinous levator ani (maroon), and insertion of the arcus tendinous fascia pelvis (teal) [15]. (Online version in colour.)

mesh convergence study (as penalty is mesh-dependent). The fetal head displacement occurred linearly over 10 000 s (2.78 h) with automatically adjusted time steps ranging from 1×10^{-05} to 1000 s. The analysis was dynamic so that temporal evolution could be studied, and all tissues were given the same density value. Numerical damping was employed to eliminate elastic wave propagation/amplification by adjusting the Newmark time integration parameters β and γ to 1 and 2, respectively. Although density can influence dynamic simulations, mass-scaling by five orders of magnitude in preliminary trials resulted in stretch ratio differences of less than 1% in corresponding anatomical regions. This indicated that these simulations were slow enough that density was not meaningfully influencing results of interest. All simulations were performed using FEBio v.2.5 (University of Utah, Salt Lake City, UT, USA).

To answer the research question motivating this study, in addition to the Included Model generated using the above methods, an Omitted Model was created with the same geometry, material properties and boundary conditions, but the influence of the superficial perineal structures (the bulbocavernosus, ischiocavernosus, and deep and superficial transverse perinei muscles, and their connective tissues) was removed. This only required the removal of all contact conditions assigned to these structures and the springs connected to them, so none of the geometries or meshes were altered, allowing for a direct comparison between models. The fetal head and maternal musculature behaved as if these superficial structures, although visible, were not physically there. This ensured that the contribution of these structures specifically was the only difference between the two models, allowing us to determine where the superficial perineal structures alone notably influence the outcomes of this childbirth simulation. As 5% is the approximate error associated with the mesh density used, differences of 10% (twice that error) or greater between models were considered meaningful. The Omitted Model is meant to represent the majority of existing childbirth models as in these models the levator ani are the only maternal muscles resisting fetal head motion during simulated vaginal delivery [11,16–19].

2.4. Data analysis

First principal Lagrangian strain versus time data were generated for both models using PostView v1.9.1 (University of Utah, Salt Lake City, UT, USA) to find the peak strain for the perineal body and right and left pubovisceral muscle entheses individually, only considering time points before any non-physiological motion of the coccyx or musculature occurred due to elastic recoil after fetal head crowning. Because the mesh was not altered to create the Omitted Model, the exact same elements could be sampled from both models to obtain strain values of identical anatomical regions. These strains were converted to stretch ratio values and per cent differences calculated to directly compare the Included and Omitted models.

The positions of the fetal head vertex (the leading portion of the head during delivery) and perineal body centroid were measured in PostView and analysed in Wolfram Mathematica Student Edition v11.0.0 (Wolfram Research, Inc., Champaign, IL, USA) using a custom code which allowed for the generation of displacement versus time plots. Using these displacements, the angle of progression was calculated at each available time point for both models from the onset of the second stage of labour ($t = 0$ in these simulations) to fetal head crowning (defined as the instant of maximum perineal body strain). Angle of progression is a two-dimensional angle between the midsagittal, long (or semi-major) axis of the ellipse-shaped pubic symphysis and a line connecting

Table 1. The maximum average stretch ratio value at each anatomical site of interest and the corresponding per cent differences when looking from the Omitted Model to the Included Model.

anatomical location	Omitted Model stretch values	Included Model stretch values	per cent difference (%)
perineal body	1.98	4.10	+107
right pubovisceral muscle	1.93	1.74	−9.84
left pubovisceral muscle	2.20	1.88	−14.6

the inferior end of this axis to the vertex of the fetal skull measured at approximately the midsagittal plane [20,21]. This has been shown to be a more reliable, robust method for measuring fetal head progression during vaginal delivery and easier to define within a finite-element model than fetal head stations [20,21]. In this study, the concept of the angle of progression was also applied to the perineal body, where the first line is still the long axis of the pubic symphysis but the second extends to the centroid of the perineal body instead of the fetal head. This served as a repeatable measure to describe and compare perineal body movement within the midsagittal plane during simulations of vaginal delivery.

3. Results

In the Included Model, which incorporates the superficial perineal structures, the perineal body experienced higher and the pubovisceral muscle entheses lower stretch values in comparison to those in the Omitted Model. The fetal head paths in both models were identical until the point of maximum perineal body strain; however, in the Included Model, the path is longer as crowning occurred at a later time point due to the longer delivery time. The path of the perineal body in the two models differed after the fetal head made initial contact with the levator hiatus. Specifically, the perineal body of the Included Model reached a larger peak inferior displacement and a larger peak and final angle of progression, accounting for the increased stretch values in that region.

From the Omitted to the Included Model, the changes in stretch were+107% in the perineal body, −9.84% in the right pubovisceral muscle and −14.6% in the left pubovisceral muscle (table 1). The Omitted Model had maximum stretch values of 1.98, 1.93 and 2.20 in the perineal body, left pubovisceral muscle and right pubovisceral muscle, respectively, while corresponding maximal stretch values were 4.10, 1.74 and 1.88 in the Included Model (table 1). The differences in the stretch values in the perineal body and left pubovisceral muscle exceed our ±10% threshold while the difference between the right pubovisceral muscles nearly reaches it.

Because the superior–inferior displacement of the fetal head was a prescribed boundary condition, the fetal head paths were the same until the Omitted Model reached the time of maximum perineal body strain despite the freedom given in the anterior–posterior and mediolateral directions (figure 5*a*,*b*). This time point arrived notably sooner in the Omitted Model (at $t \approx 4844$ s with an angle of progression of 192.3°) compared to the Included Model (at $t \approx 6146$ s with an angle of 203.3°), but that was the only notable difference (figure 5*c*). Adding the superficial perineal structures resulted in an 11.0°, or+5.71%, increase in the final fetal head angle of progression in the Included Model (figure 5*d*). Although these fetal head angle of progression differences were not significant, the +26.9% difference in the final fetal head superior–inferior displacement was significant. Mediolateral (x) displacements, which represent a deviation from the midsagittal plane, were minimal (for both the fetal head and the perineal body) and fetal head superior–inferior displacements were prescribed; therefore, these specific results are not shown.

As expected, until the fetal head engaged the levator hiatus, the displacement and angle of progression curves for the perineal bodies were almost identical. Following this contact, the perineal body paths diverged. The anterior–posterior displacements only differed in timing as the slopes and magnitudes were otherwise quite similar (figure 6*a*). Although the fetal head path was not significantly altered, the perineal body was forced to inferiorly displace 7.8 mm, or+72.5% (greater than our ±10% threshold), further at its peak in the Included Model due to the presence of the superficial perineal structures (figure 6*b*). This corresponds with an angle of progression 14.6°, or+8.00%, larger in the Included Model (figure 6*c*). The peak superior–inferior displacement and maximum angle of progression of the Included Model were 18.5 mm and 196.9°, respectively, while those of the Omitted Model were 10.7 mm and 182.3°. For the perineal body in each model to reach the same final anterior–posterior and superior–inferior displacement, the perineal body in the Included Model had to deform more in the inferior direction (figure 6*d*). This resulted in the higher stretch ratio, superior–inferior displacement and angle of progression values observed in the Included Model.

4. Discussion

These results refute the stated hypothesis, suggesting that superficial perineal structures play a critical role in maternal birth injury pathophysiology and should be included in future computational models. This work also supports that the perineal body is more vulnerable to injury than previously appreciated, which is consistent with the relatively large quantity of perineal tears observed clinically [5,22].

Inclusion of the superficial perineal structures resulted in higher stretch values in the perineal body and lower values in the pubovisceral muscle, indicating that the Omitted Model, and those with geometries like it, underestimate perineal body and overestimate pubovisceral muscle stretch. The per cent differences imply that this perineal body underestimation is much more severe than the pubovisceral muscle overestimation. When maternal musculature is modelled as a simple, sling-like shape, the levator ani—specifically the pubovisceral muscle entheses—take on a higher proportion of the load. By contrast, when the superficial perineal structures are present to decrease urogenital hiatus size and restrict the perineal body, as demonstrated in the Included Model, the perineal body can no longer move as easily and

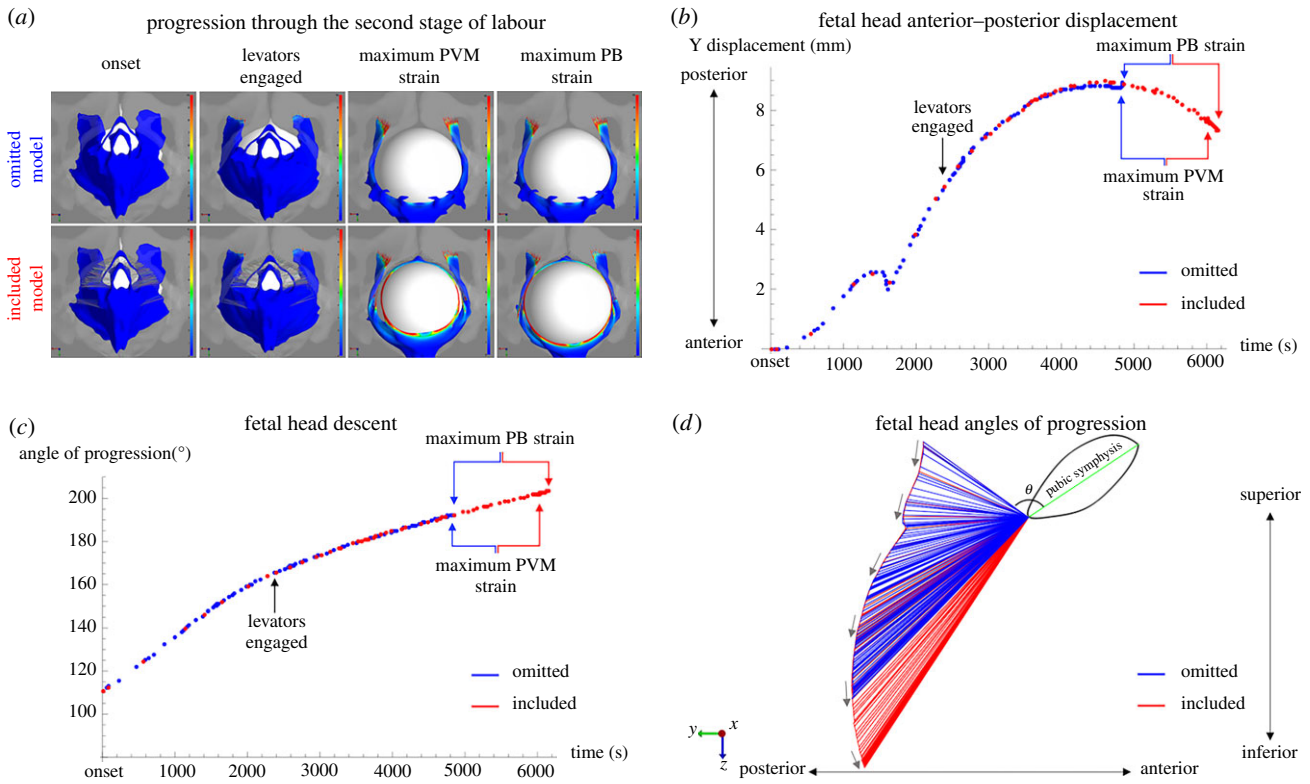

Figure 5. (*a*) Screenshots from both the Omitted and Included models at the onset of the second stage of labour (far left column), when the fetal head engages the levator hiatus (second column), average time point between maximum right and left pubovisceral muscle (PVM) strains (third column), and maximum perineal body (PB) strain (far right column). (*b*) A plot of fetal head anterior–posterior displacements with labelled arrows pointing to the instances shown in (*a*). (*c*) A labelled plot of the angle of progression values for the fetal head. (*d*) A visualization of those angles in the midsagittal plane. The arrows are guides pointing away from the onset of labour towards the moment of maximum PB strain, θ represents the initial angle of progression, and the green line emphasizes the long axis of the pubic symphysis. (Online version in colour.)

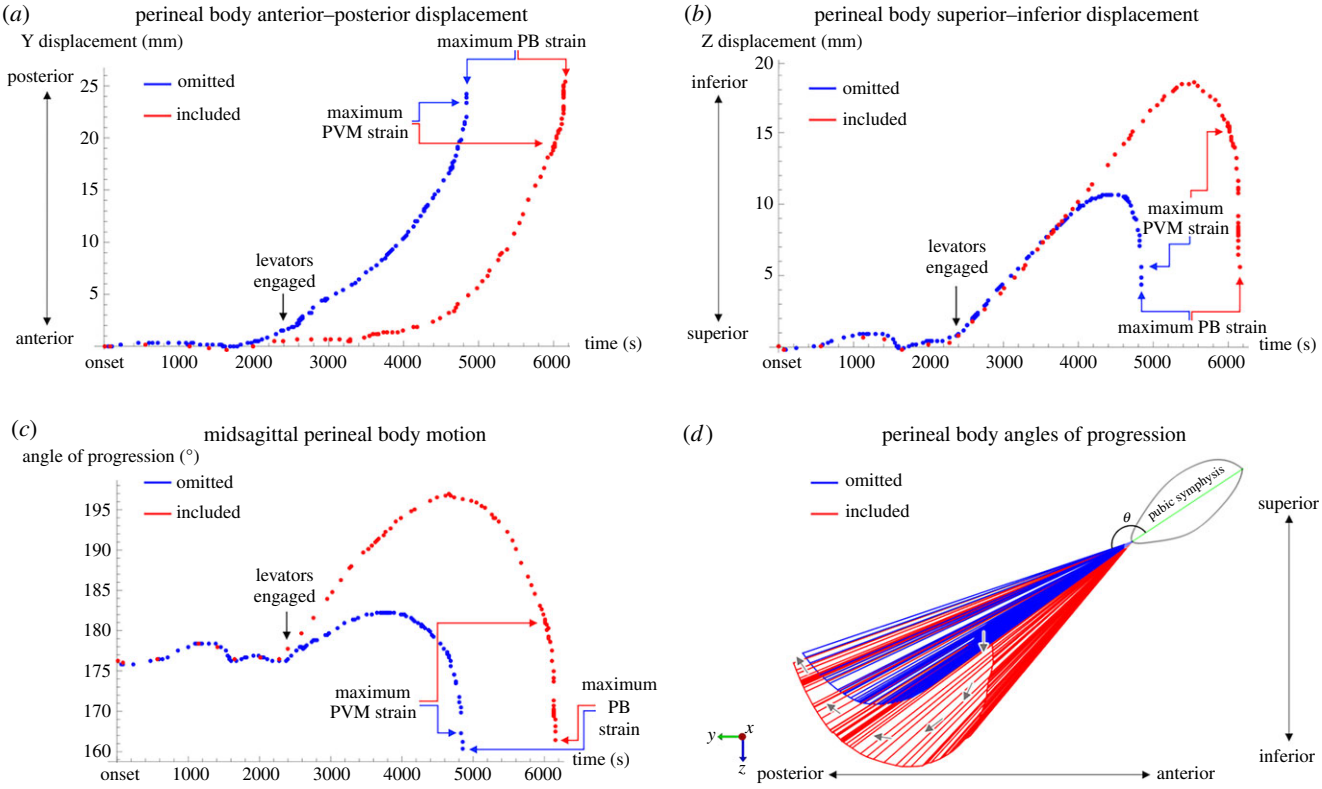

Figure 6. (*a*) A plot of perineal body (PB) anterior–posterior displacements with the same timepoints from figure 5 labelled. (*b*) A labelled plot of perineal superior–inferior displacements. (*c*) A labelled plot of the modified angle of progression values for the centroid of the PB. (*d*) A visualization of those angles in the midsagittal plane. The arrows are guides pointing away from the onset of labour towards the moment of maximum PB strain, θ represents the initial angle of progression, and the green line emphasizes the long axis of the pubic symphysis. (Online version in colour.)

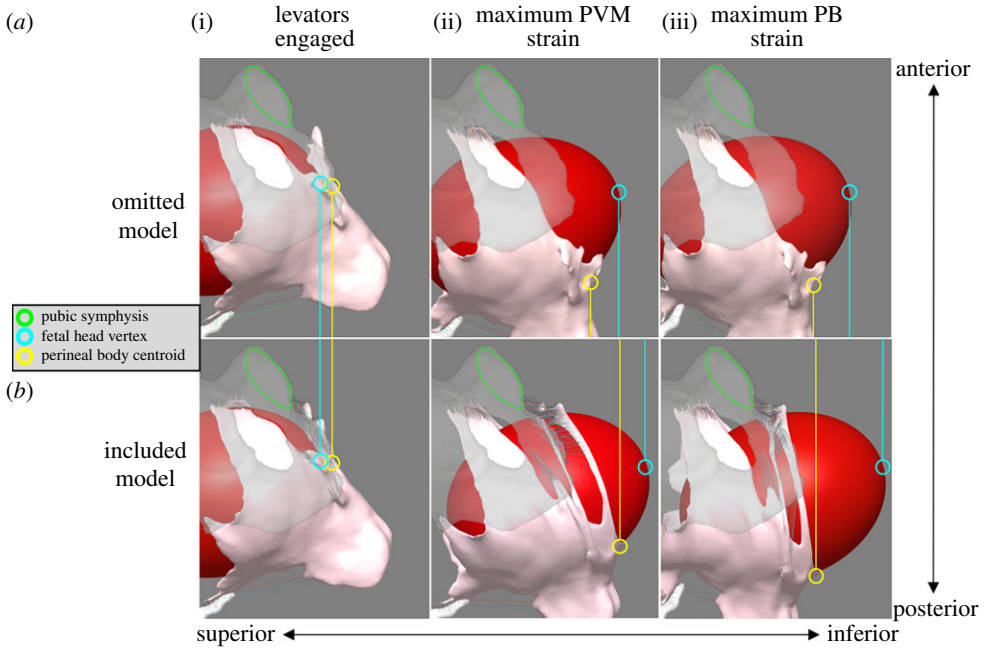

Figure 7. Screenshots from both the Omitted (*a*) and Included (*b*) models at the moment the fetal head engages the levator hiatus (*a*(i), *b*(i)), the average time point between maximum right and left pubovisceral muscle (PVM) strains (*a*(ii), *b*(ii)), and the moment of maximum perineal body (PB) strain (*a*(iii), *b*(iii)). The pubic symphysis (outlined in green) serves as a point of reference. The differences in the superior–inferior positions of the fetal head vertex (circled in blue) and PB centroid (circled in yellow) between models are emphasized with vertical lines coming from each. (Online version in colour.)

must stretch instead. This is more similar to what is observed *in vivo* as the perineum stretches drastically while its motion is restricted during fetal head crowning.

These stretch values are reasonable compared to previous studies (with models similar to the Omitted Model) as values range from 1.6 to 3.5 in the levator ani [15]. The perineal body in the Included Model surpasses this range, which could potentially be explained by the variation in perineal body location across childbirth models. The perineal body is commonly described as the fibromuscular structure between the anus and vagina and superficial to the pelvic diaphragm, but its exact boundary and composition are widely debated [2,23]. Studies have determined that it is comprised of three layers but do not agree on the location and makeup of each layer [23,24]. When childbirth models only include structures at the same depth as the levator ani, they are only including the deepest layer of the perineal body, if any true layer at all [23,24]. The Included Model contains the thickness of more, if not all three, layers as well as corresponding connective tissue attachments. This could explain the increased perineal body stretching as, in addition to the levator ani, the superficial perineal structures were also pulling it in opposing directions.

The fetal head in both models started at an angle of progression of 100°, but at the moment of fetal head crowning—defined here as the point of maximum perineal body strain, as in previous studies—the Included Model had a larger value [20,21,25]. The superficial perineal structures increased the final fetal head angle of progression, indicating that the soft tissues in the Included Model were pushed further to reach an analogous moment of fetal head crowning. This is corroborated by the perineal body data.

The perineal body in the Included Model was forced to stretch and inferiorly displace further to reach a similar final anterior–posterior and superior–inferior displacement as the Omitted Model (figure 7). Although both models reach similar final displacements, the Included Model took longer to do so. This acts as a form of validation as the anatomical function of the superficial perineal structures *in vivo* is to restrict caudal, or anterior–posterior, motion of the perineal body [10]. These structures forced the perineal body to stretch further by creating tension that restricted its anterior–posterior motion as it was being pushed posteriorly by the fetal head. When the superficial perineal structures were not present, it was easy for that tissue to be pushed out of the way (as demonstrated by the smaller perineal body angle of progression values in the Omitted Model). Although the angle of progression is typically used to assess fetal head progression, it was employed here as a robust method for measuring and a basis for a more quantitative evaluation of midsagittal perineal body movement during the second stage of labour that could be used in future computational and experimental studies.

As a first attempt to quantify the importance of superficial perineal structures in finite-element models of vaginal delivery, this study has several limitations. The maternal geometry was from an older, parous, female cadaver, which likely does not appropriately represent a woman at full-term. All maternal muscles were continuous, hyper-elastic, passive, lacked fibre directions and assigned the same, simplified material properties meant to serve as initial estimates for future experiments. While many of these muscles are continuous anatomically, there are identifiable boundaries, varying fibre orientations, and possibly varying material properties in women at full-term, making it unclear how stresses are transferred *in vivo* during delivery. The fetal head was small, rigid and rotation was restricted, although the small size was not considered a substantial limitation as the fetal head moulds during vaginal delivery *in vivo* in order to fit through the birth canal by reducing the fetal head circumference. This model does not incorporate fetal head moulding, so using measurements of a fetal head at term would have resulted in an overestimation of stretch ratio values throughout the simulated delivery. Work is currently being done to overcome these limitations, but, as they affect

both models equally, it is assumed that the direct comparisons reported here are minimally affected.

5. Conclusion

After thorough observation and analysis, it is believed that the Included Model in this study provides a better gross impression of the maternal geometry and biomechanics in response to the passage of the fetal head during the second stage of labour. These results suggest that the superficial perineal structures likely warrant more focus in future computational and experimental studies of childbirth biomechanics than given previously.

Ethics. Use of the images of the female cadaver from the Visible Human Project (US National Library of Medicine, Bethesda, MD, USA) required a licence distributed by the Department of Health & Human Services but not consent or IRB approval.

Data accessibility. The datasets supporting this article have been uploaded as part of the electronic supplementary material.

Authors' contributions. M.R. segmented the maternal geometries, created the finite-element models and ran the simulations, conducted data analyses, generated tables and figures, participated in the conception/design of the study and drafted the manuscript; P.A. participated in the conception/design of the study and critically revised the manuscript and figures; S.M. participated in the conception/design of the study and critically revised the manuscript; R.D. participated in the conception/design of the study and critically revised the manuscript; and S.A. coordinated the study, participated in the conception/design of the study and critically revised the manuscript. All authors gave final approval for publication and agree to be held accountable for the work performed therein.

Competing interests. We declare we have no competing interests.

Funding. This work was supported by the National Science Foundation (award no. 1511504 and GRFP grant no. 1747452) and the National Institute of Health (RO1HD03383).

Acknowledgements. We would like to recognize the National Library of Medicine for access to the Visible Human Project image database.

References

1. Wu JM, Vaughan CP, Goode PS, Redden DT, Burgio KL, Richter HE, Markland AD. 2014 Prevalence and trends of symptomatic pelvic floor disorders in U.S. women. *Obstet. Gynecol.* **123**, 141–148. (doi:10.1097/AOG.0000000000000057)
2. Herschorn S. 2004 Female pelvic floor anatomy: the pelvic floor, supporting structures, and pelvic organs. *Rev. Urol.* **6**, S2–S10. (doi:10.1007/978-3-662-05445-1_5)
3. Jing D, Ashton-Miller JA, DeLancey JOL. 2012 A subject-specific anisotropic visco-hyperelastic finite element model of female pelvic floor stress and strain during the second stage of labor. *J. Biomech.* **45**, 455–460. (doi:10.1016/j.jbiomech.2011.12.002)
4. DeLancey JOL, Kearney R, Chou Q, Speights S, Binno S. 2003 The appearance of levator ani muscle abnormalities in magnetic resonance images after vaginal delivery. *Obstet. Gynecol.* **101**, 46–53. (doi:10.1016/S0029-7844(02)02465-1)
5. Samuelsson E, Ladfors L, Lindblom BG, Hagberg H. 2002 A prospective observational study on tears during vaginal delivery: occurrences and risk factors. *Acta Obstet. Gynecol. Scand.* **81**, 44–49. (doi:10.1046/j.0001-6349.2001.10182.x)
6. Ashton-Miller JA, DeLancey JOL. 2007 Functional anatomy of the female pelvic floor. *Ann. NY Acad. Sci.* **1101**, 266–296. (doi:10.1196/annals.1389.034)
7. Silva MET, Oliveira DA, Roza TH, Brandao S, Parente MPL, Mascarenhas T, Natal Jorge RM. 2015 Study on the influence of the fetus head molding on the biomechanical behavior of the pelvic floor muscles, during vaginal delivery. *J. Biomech.* **48**, 1–6. (doi:10.1016/j.jbiomech.2014.11.017)
8. Vila Pouca MCP, Ferreira JPS, Oliveira DA, Parente MPL, Mascarenhas T, Natal Jorge RM. 2018 On the effect of labour durations using an anisotropic visco-hyperelastic-damage approach to simulate vaginal deliveries. *J. Mech. Behav. Biomed. Mater.* **88**, 120–126. (doi:10.1016/j.jmbbm.2018.08.011)
9. Ferreira JPS, Parente MPL, Jabareen M, Natal Jorge RM. 2017 A general framework for the numerical implementation of anisotropic hyperelastic material models including non-local damage. *Biomech. Model. Mechanobiol.* **16**, 1119–1140. (doi:10.1007/s10237-017-0875-9)
10. DeLancey JO. 1999 Structural anatomy of the posterior pelvic compartment as it relates to rectocele. *Am. J. Obstet. Gynecol.* **180**, 815–823. (doi:10.1016/S0002-9378(99)70652-6)
11. Li X, Kruger JA, Nash MP, Nielsen PMF. 2010 Modeling childbirth: elucidating the mechanisms of labor. *Wiley Interdiscip. Rev. Syst. Biol. Med.* **2**, 460–470. (doi:10.1002/wsbm.65)
12. Chitty LS, Altman DG, Henderson A, Campbell S. 1994 Charts of fetal size: 2. Head measurements. *BJOG: Int. J. Obstet. Gynaecol.* **101**, 35–43. (doi:10.1111/j.1471-0528.1994.tb13007.x)
13. Lubchenco LO, Hansman C, Boyd E. 1966 Intrauterine growth in length and head circumference as estimated from live births at gestational ages from 26 to 42 weeks. *Pediatrics* **37**, 403–408.
14. Fenton TR, Kim JH. 2013 A systematic review and meta-analysis to revise the Fenton growth chart for preterm infants. *BMC Pediatr.* **13**, 59. (doi:10.1186/1471-2431-13-59)
15. Hoffman BL, Schorge JO, Bradshaw KD, Halvorson LM, Schaffer JI, Corton MM (eds) 2016 *Williams gynecology*, 3rd edn. New York, NY: McGraw-Hill Education.
16. Tracy PV, DeLancey JO, Ashton-Miller JA. 2016 A geometric capacity–demand analysis of maternal levator muscle stretch required for vaginal delivery. *J. Biomech. Eng.* **138**, 21001. (doi:10.1115/1.4032424)
17. Lien K-C, Mooney B, DeLancey JOL, Ashton-Miller JA. 2004 Levator ani muscle stretch induced by simulated vaginal birth. *Obstet. Gynecol.* **103**, 31–40. (doi:10.1097/01.AOG.0000109207.22354.65)
18. Parente MPL, Jorge RMN, Mascarenhas T, Fernandes AA, Martins JAC. 2007 Deformation of the pelvic floor muscles during a vaginal delivery. *Int. Urogynecol. J.* **19**, 65–71. (doi:10.1007/s00192-007-0388-7)
19. Li X, Kruger JA, Nash MP, Nielsen PMF. 2011 Anisotropic effects of the levator ani muscle during childbirth. *Biomech. Model. Mechanobiol.* **10**, 485–494. (doi:10.1007/s10237-010-0249-z)
20. Levy R, Zaks S, Ben-Arie A, Perlman S, Hagay Z, Vaisbuch E. 2012 Can angle of progression in pregnant women before onset of labor predict mode of delivery? *Ultrasound Obstet. Gynecol.* **40**, 332–337. (doi:10.1002/uog.11195)
21. Bibbo C, Rouse CE, Cantonwine DE, Little SE, McElrath TF, Robinson JN. 2018 Angle of progression on ultrasound in the second stage of labor and spontaneous vaginal delivery. *Am. J. Perinatol.* **35**, 413–420. (doi:10.1055/s-0037-1608633)
22. Harkin R, Fitzpatrick M, O'Connell PR, O'Herlihy C. 2003 Anal sphincter disruption at vaginal delivery: is recurrence predictable? *Eur. J. Obstet. Gynecol. Reprod. Biol.* **109**, 149–152. (doi:10.1016/S0301-2115(03)00008-3)
23. Larson KA, Yousuf A, Lewicky-Gaupp C, Fenner DE, Delancey JOL. 2010 Perineal body anatomy in living women: 3-dimensional analysis using thin-slice magnetic resonance imaging. *Am. J. Obstet. Gynecol.* **203**, 494-e15–494.e21. (doi:10.1016/j.ajog.2010.06.008)
24. Shafik A, Sibai O, Shafik AA, Shafik IA. 2007 A novel concept for the surgical anatomy of the perineal body. *Dis. Colon Rectum* **50**, 2120–2125. (doi:10.1007/s10350-007-9064-8)
25. Ashton-Miller JA, Delancey JOL. 2009 On the biomechanics of vaginal birth and common sequelae. *Annu. Rev. Biomed. Eng.* **11**, 163–176. (doi:10.1146/annurev-bioeng-061008-124823)